Glide-symmetric fully-metallic Luneburg lens for 5G Communications at Ka-band

Oscar Quevedo-Teruel, Jingwei Miao, Martin Mattsson, Astrid Algaba-Brazalez, Martin Johansson, Lars Manholm

Glide-symmetric fully-metallic Luneburg lens for 5G Communications at Ka-band

Oscar Quevedo-Teruel, *Senior Member, IEEE,* Jingwei Miao, Martin Mattsson, Astrid Algaba-Brazalez, Martin Johansson, *Senior Member, IEEE,* and Lars Manholm

***Abstract*—Here, we propose a fully-metallic implementation of a Luneburg lens operating at Ka-band with potential use for 5G communications. The lens is implemented with a parallel plate that is loaded with glide-symmetric holes. These holes are employed to produce the required equivalent refractive index profile of a Luneburg lens. Glide symmetry and inner metallic pins are employed to increase the equivalent refractive index. The lens is fed with rectangular waveguides designed to match the height of the parallel plate, and it is ended with a flare to minimize the reflections.**

***Index Terms*—Higher symmetries, glide symmetry, periodic structures, Luneburg lens, fully-metallic lens, Ka-band, 5G.**

I. Introduction

The increased demand of wireless data transfer with short delays is changing our communications to a new paradigm named 5G. In order to fulfill the requirements of 5G, the operational frequency must be increased [1], being Ka-band one of the bands under consideration [2]. Specifically, a center frequency of 28 GHz with a 20% bandwidth has been considered in previous works [3]. Here, we propose an antenna solution that makes use of a Luneburg lens with a potential use as an access antenna at 28 GHz.

When the frequency increases, the path loss becomes higher, so directive antennas with steerable angle of radiation are needed [4]. In order to increase the directivity of an antenna, arrays, reflectors or lenses can be employed. At high frequency, the feeding network of arrays may be complicated, and consequently the losses will be high [5], [6]. On the other hand, electronically-reconfigurable reflectors are difficult to implement [7], [8]. Lens antennas can be bulky, and have high losses due to the propagation in dielectric materials and reflections in the material transitions [9].

Here, we propose a two-dimensional fully-metallic lens with low losses. The equivalent refractive index of the lens is achieved with holes loading a parallel plate configuration. In order to increase the equivalent refractive index produced by the holes, they are loaded with metallic pins and tailored in a glide-symmetric configuration.

Glide symmetry was studied in the 60s and 70s for one-dimensional propagation and leaky-wave antennas [10], [11], [12]. A periodic structure is glide-symmetric if it is invariant after a translation and a mirroring. The research on glide-symmetric structures has been recently revitalized with the new discovery of valuable electromagnetic properties for practical applications [13], [14], [15]. In [16], it was demonstrated that glide symmetry can be employed to increase the equivalent refractive index of two-dimensional structures, as well as to reduce their dispersion and anisotropy. More recently, glide-symmetric structures have demonstrated to be a suitable solution to increase the bandwidth of electromagnetic bandgaps (EBG) [17]. These EBGs have been proposed as a cost-efficient solution for reducing the leakage in gap-waveguide technology [18] and in transitions between waveguides [19]. Glide symmetry has been also applied to reduce the dispersion of slotted metasurfaces [20] and transmission lines [21], [22].

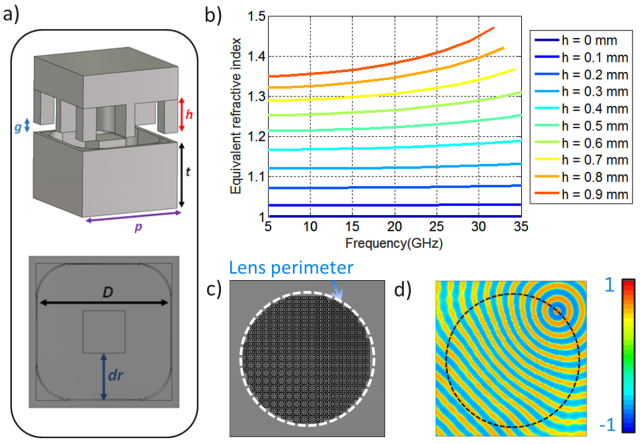

Fig. 1. a) Unit cell under study: A fully-metallic configuration with pin-loaded holes on top and bottom following a two-dimensional glide symmetry. b) Equivalent refractive index for g = 3 mm, t = 2.9 mm, D = 2.9 mm, dr = 1 mm and p = 3.2 mm, while the h is modified. c) Bottom layer of the designed Luneburg lens with holes of different height, h. d) Simulated normalized electric field in the air gap between top and bottom layers.

II. Luneburg lens design

Luneburg lenses have a response that is very suitable for antenna designs [23], [24], [25], [26]. A Luneburg lens is a rotationally-symmetric graded-index lens that transforms a point source (cylindrical or spherical wave) into a plane wave at the opposite direction in which it is fed [27]. One excellent characteristic of Luneburg lenses is that they finalise with a refractive index of 1 at their contour. Therefore, a perfect matching with free-space is achieved and no reflections at the borders are expected. Reflections in a Luneburg lens are only

O. Quevedo-Teruel, J. Miao and M. Mattsson are with the Department of Electromagnetic Engineering at KTH Royal Institute of Technology, SE-10044, Stockholm, Sweden.

A. Algaba-Brazalez, M. Johansson and L. Manholm are with Ericsson Research at Ericsson AB, Gothenburg, Sweden.

Manuscript received Month XX, 2017; revised Month XX, 2017.

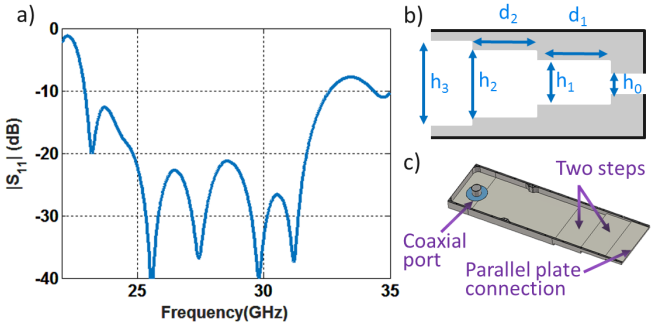

Fig. 2. a) S_{11} parameter for transition between coaxial connector and the end of the waveguide. The parameters are d_1 = 3.92 mm, d_2 = 4.23 mm, h_0 = 0.3 mm, h_1 = 0.62 mm, and h_2 = 1.32 mm and h_3 = 1.778 mm b) Side view of the transtition. c) Feeding configuration: Waveguide fed with a 2.92 mm coaxial connector, with a pin height of 1.22 mm.

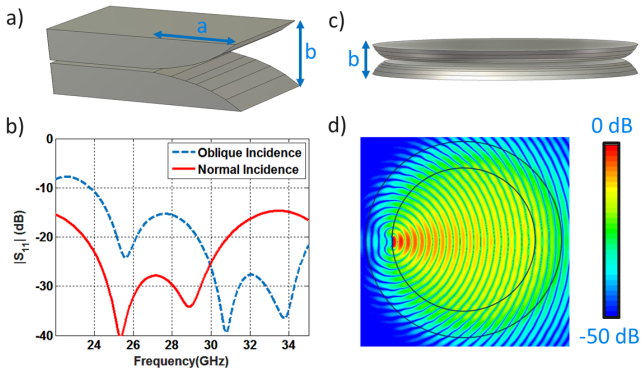

Fig. 3. a) One-dimensional discretized flare scheme for optimization. b) S_{11} parameter for the optimized one-dimensional flare. c) Parallel plate without lens and ended by the designed flare. d) Simulated electric field distribution for the configuration in c) at 28 GHz.

produced at the transitions between materials defined by the required discretization in a practical implementation.

Although the original idea of Luneburg was to implement a dielectric lens, dielectric materials produce high losses when the frequency increases. To overcome this limitation, non-Euclidean transformations were proposed to produce fully-metallic solutions [28], [29], and particularly implemented in the Ka-band for satellite communications [30]. A second possibility consists of using periodic structures, such as metallic pins with different heights to tailor the required refractive index [31], [32], [33]. Differently to these works, we propose here the use of periodic glide-symmetric holes as initially proposed in [16]. Holey structures are easy to mill, and more cost-effective than pin-type solutions [34], [35]. However, holes require small distances between plates to provide a sufficient increase of the equivalent refractive index.

Our proposed periodic structure is represented in Fig. 1.a). In order to increase the distance between parallel plates, the refractive index provided by conventional holes was enhanced by using vertical metallic inclusions (pins), which act as loads inside the holes, as previously proposed in [36], [37]. After optimization, and establishing an air gap of g = 0.3 mm, the selected parameters are t = 2.9 mm, D = 2.9 mm, dr = 1 mm, and p = 3.2 mm. The air gap plays an important role, since it will define the bandwidth of operation of the unit cell [38]. Keeping in mind the manufacturing of the lens will be done with a milling machine, the outer radius of the milled corners is considered to be 0.75mm. This will avoid that the machine stops in the corners, which could cause some problems with extra milling while stationary. Therefore, the center of the drill will follow a smooth curve with a radius of $dr/4$ = 0.25mm.

To tune the equivalent refractive index from 1 at the edge to 1.4 at the center, the height (h) is changed from 0 to 0.9 mm, obtaining the dispersion response shown Fig. 1.b). A Luneburg lens can be mimicked by using different heights of holes at the different positions as represented in Fig. 1.c), obtaining the response shown in Fig. 1.d). To demonstrate the performance of the lens, a cylindrical wave is excited at the top-right of the lens, and it is transformed into a plane wave in the bottom-left.

III. Feeding and Flare Design

In order to use a Luneburg lens as an antenna, a feeding network is needed. Each of the feeding points of the network will produce a plane wave at different directions. Since our Luneburg lens is designed in a parallel plate, the feedings are waveguides that are adapted to the height between the metallic layers. These waveguides were optimized with a two-stage stepped height transition from 1.78 mm height to 0.3 mm (lens gap) to minimize the reflections from a standard 2.92 mm coaxial connector. The transition is illustrated in Fig. 2.b,c). The obtained reflection coefficient is plotted in Fig. 2.a) with a matching below -20 dB in the bandwidth of interest.

After a plane wave is created at the opposite side of the lens from which it is fed, the electromagnetic waves must be efficiently radiated. However, the distance between the parallel plates is thin (0.3 mm), so an abrupt ending will produce elevated reflections. Therefore, a flare must be designed to reduce the reflections at the end of the antenna [39], [40], [41]. The design of the flare was done with a one-dimensional optimization based on 6 points, as illustrated in Fig. 3.a), assuming a final aperture height of b = 6.36 mm ($\simeq 0.65\ \lambda_0$.) and a length a = 20.91 mm. The optimized flare produces less than -15 dB in main and oblique incidences as illustrated in Fig. 3.b). The flare was designed to cover an angular range of ± 50 °. Larger angular scanning will reduce the gain of antenna at the extreme angles [42], [43]. In Fig. 3.c), a parallel plate (without lens inside) with a rotationally-symmetric flare is illustrated, and the resulting electric field when it is fed with waveguide port is plotted in Fig. 3.d).

By adding one feeding waveguide to the Luneburg lens and applying the flare at the opposite direction as illustrated in Fig. 4.a), the obtained electric field distribution is as plotted in Fig. 4.b). The Luneburg lens is fed from the right side, and a plane wave is formed at the left side, i.e. a very directive beam is radiating in the opposite direction of the feeding.

IV. Experimental Results

In Fig. 5.a,b), a photo of the bottom layer of the final antenna is illustrated. The prototype has been measured in

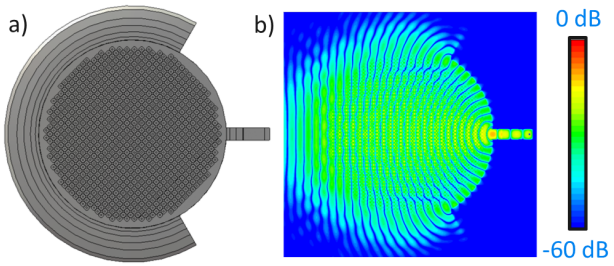

Fig. 4. a) Scheme of the lens antenna with a centered feed. b) Simulated electric field distribution inside the lens.

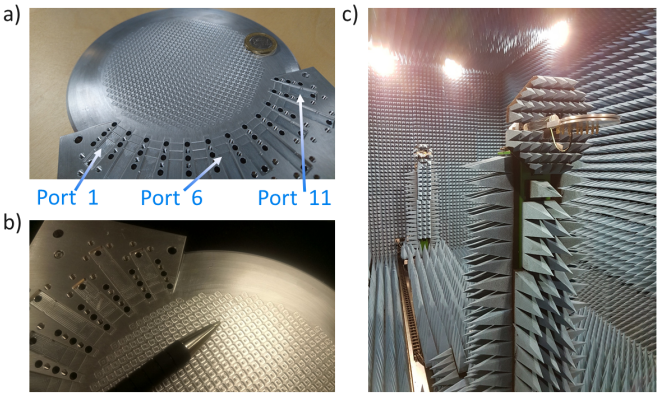

Fig. 5. a) Photo of the bottom layer of the manufactured Luneburg lens with numbered ports. b) Zoom of the lens. c) Measurement configuration at the anechoic chamber at KTH Royal Institute of Technology.

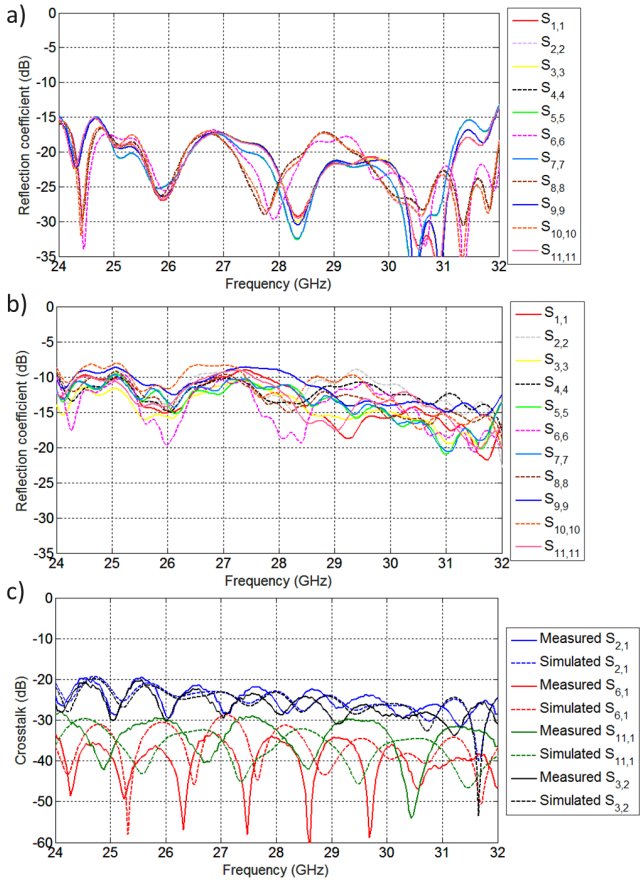

Fig. 6. S-parameters of the antenna. a) Simulated reflection coefficients. b) Measured reflection coefficients. c) Measured and simulated coupling coefficients.

the anechoic chamber facilities at KTH Royal Institute of Technology as shown in Fig.5.c). The simulated and measured S-parameters are represented in Fig. 6. The mutual coupling between ports is lower than -20 dB. On the other hand, the reflection coefficient has been increased with respect to the simulated results. Although the results are acceptable, in some frequency regions, the S_{11} is slightly higher than -10 dB. These discrepancies are due to the tolerances in the manufacturing of the waveguide-to-parallel plate transition, and the length of the inner conductor of the ports that were slightly different to the nominal specified by the manufacturer. The parameters that most affect the matching are the relative position of the probe and the height of the inner conductor [38]. The power efficiency of the antenna is 88%. The detailed power losses were simulated and are illustrated in Fig. 7. The radiation patterns are shown in Fig. 8.b-d) for three different frequencies, which correspond to the lower, center, and higher frequencies of operation. The measurements were repeated after disassembling and reassembling the lens to demonstrate their repeatability. Good agreement between measurements and simulations was achieved. The measurements demonstrate a stable gain with respect to the angle of scanning. A higher level of overlapping between beams could be achieved by placing the feedings closer to each other, although this would lead to an increase in the coupling between ports [44], [45].

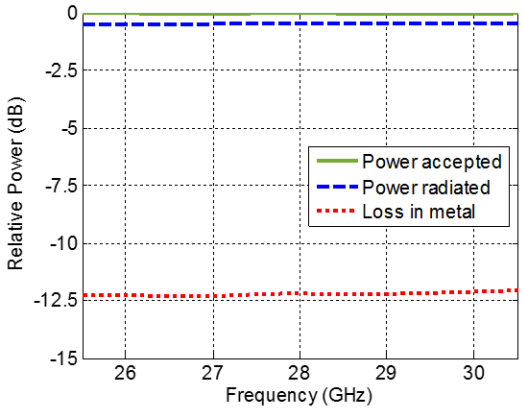

Fig. 7. Evaluation of the losses for the complete antenna.

V. Conclusion

Here, we have proposed a fully-metallic Luneburg lens for 5G communications at the Ka-band. The lens antenna provides a steerable radiation pattern with high directivity, low side lobe levels and high radiation efficiency. The lens is designed with pin-loaded holes possessing glide symmetry. Glide symmetry is employed to increase the equivalent refractive index of the periodic structure, while maintaining a thick enough air gap

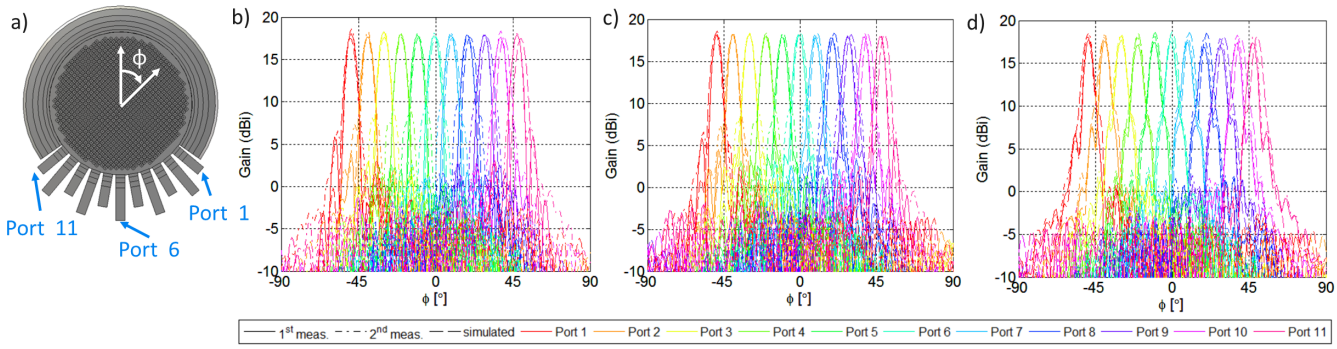

Fig. 8. a) Configuration and port numbers. b) Radiation patterns at 25.2 GHz. c) Radiation pattern at 28 GHz. d) Radiation pattern at 30.8 GHz.

between layers that ensures good tolerances in the manufacturing. The lens is fed with waveguides and it is ended with a flare to reduce the reflections at the edges. The measurements demonstrate the feasibility of the solution, although an increase of the S_{11} with respect to the simulations has been detected. This effect is due to manufacturing tolerances, which is a crucial aspect in the practical implementation of this type of antenna.

ACKNOWLEDGMENT

The authors would like to thank to Jesper Freiberg for his support in the manufacturing and testing of the prototype.

REFERENCES

[1] S. Parkvall, E. Dahlman, A. Furuskar, and M. Frenne, "NR: The new 5G radio access technology," *IEEE Communications Standards Magazine*, vol. 1, no. 4, pp. 24–30, Dec 2017.

[2] D. Liu, X. Gu, C. W. Baks, and A. Valdes-Garcia, "Antenna-in-package design considerations for Ka-band 5G communication applications," *IEEE Trans. Antennas Propag.*, vol. 65, no. 12, pp. 6372–6379, Dec 2017.

[3] K. Kibaroglu, M. Sayginer, and G. M. Rebeiz, "A low-cost scalable 32-element 28-GHz phased array transceiver for 5G communication links based on a 2x2 beamformer flip-chip unit cell," *IEEE J. Solid-State Circuits*, 2018.

[4] Y. Wang, J. Li, L. Huang, Y. Jing, A. Georgakopoulos, and P. Demestichas, "5G mobile: Spectrum broadening to higher-frequency bands to support high data rates," *IEEE Veh. Technol. Mag.*, vol. 9, no. 3, pp. 39–46, Sept 2014.

[5] S. Shakib, H. C. Park, J. Dunworth, V. Aparin, and K. Entesari, "A highly efficient and linear power amplifier for 28-GHz 5G phased array radios in 28-nm CMOS," *IEEE J. Solid-State Circuits*, vol. 51, no. 12, pp. 3020–3036, Dec 2016.

[6] R. Garg and A. S. Natarajan, "A 28-GHz low-power phased-array receiver front-end with 360 RTPS phase shift range," *IEEE Trans. Microw. Theory Techn.*, vol. 65, no. 11, pp. 4703–4714, Nov 2017.

[7] S. K. Rao and M. Q. Tang, "Stepped-reflector antenna for dual-band multiple beam satellite communications payloads," *IEEE Trans. Antennas Propag.*, vol. 54, no. 3, pp. 801–811, March 2006.

[8] K. K. Chan and S. K. Rao, "Design of high efficiency circular horn feeds for multibeam reflector applications," *IEEE Trans. Antennas Propag.*, vol. 56, no. 1, pp. 253–258, Jan 2008.

[9] O. Quevedo-Teruel, M. Ebrahimpouri, and F. Ghasemifard, "Lens antennas for 5G communications systems," *IEEE Commun. Mag.*, 2018.

[10] P. J. Crepeau and P. R. McIsaac, "Consequences of symmetry in periodic structures," *Proc. IEEE*, vol. 52, no. 1, pp. 33–43, Jan 1964.

[11] R. Kieburtz and J. Impagliazzo, "Multimode propagation on radiating traveling-wave structures with glide-symmetric excitation," *IEEE Trans. Antennas Propag.*, vol. 18, no. 1, pp. 3–7, Jan 1970.

[12] A. Hessel, M. H. Chen, R. C. M. Li, and A. A. Oliner, "Propagation in periodically loaded waveguides with higher symmetries," *Proc. IEEE*, vol. 61, no. 2, pp. 183–195, Feb 1973.

[13] R. Quesada, D. Martín-Cano, F. J. García-Vidal, and J. Bravo-Abad, "Deep-subwavelength negative-index waveguiding enabled by coupled conformal surface plasmons," *Opt. Lett.*, vol. 39, no. 10, pp. 2990–2993, May 2014.

[14] G. Valerio, Z. Sipus, A. Grbic, and O. Quevedo-Teruel, "Accurate equivalent-circuit descriptions of thin glide-symmetric corrugated metasurfaces," *IEEE Trans. Antennas Propag.*, vol. 65, no. 5, pp. 2695–2700, May 2017.

[15] F. Ghasemifard, M. Norgren, and O. Quevedo-Teruel, "Dispersion analysis of 2-d glide-symmetric corrugated metasurfaces using mode-matching technique," *IEEE Microw. Compon. Lett.*, vol. 28, no. 1, pp. 1–3, Jan 2018.

[16] O. Quevedo-Teruel, M. Ebrahimpouri, and M. N. M. Kehn, "Ultrawideband metasurface lenses based on off-shifted opposite layers," *IEEE Antennas Wireless Propag. Lett.*, vol. 15, pp. 484–487, Dec 2016.

[17] M. Ebrahimpouri, O. Quevedo-Teruel, and E. Rajo-Iglesias, "Design guidelines for gap waveguide technology based on glide-symmetric holey structures," *IEEE Microw. Compon. Lett.*, vol. 27, no. 6, pp. 542–544, June 2017.

[18] M. Ebrahimpouri, E. Rajo-Iglesias, Z. Sipus, and O. Quevedo-Teruel, "Cost-effective gap waveguide technology based on glide-symmetric holey ebg structures," *IEEE Trans. Microw. Theory Techn.*, vol. 66, no. 2, pp. 927–934, Feb 2018.

[19] M. Ebrahimpouri, A. A. Brazalez, L. Manholm, and O. Quevedo-Teruel, "Using glide-symmetric holes to reduce leakage between waveguide flanges," *IEEE Microwave and Wireless Components Letters*, vol. 28, no. 6, pp. 473–475, June 2018.

[20] M. Camacho, R. C. Mitchell-Thomas, A. P. Hibbins, J. R. Sambles, and O. Quevedo-Teruel, "Designer surface plasmon dispersion on a one-dimensional periodic slot metasurface with glide symmetry," *Opt. Lett.*, vol. 42, no. 17, pp. 3375–3378, Sep 2017.

[21] ——, "Mimicking glide symmetry dispersion with coupled slot metasurfaces," *Appl. Phys. Lett.*, vol. 111, no. 12, p. 121603, 2017.

[22] O. Dahlberg, R. C. Mitchell-Thomas, and O. Quevedo-Teruel, "Reducing the dispersion of periodic structures with twist and polar glide symmetries," *Sci. Rep.*, vol. 7, no. 1, p. 10136, 8 2017.

[23] G. Peeler and H. Coleman, "Microwave stepped-index Luneberg lenses," *IRE Trans. Antennas Propag.*, vol. 6, no. 2, pp. 202–207, April 1958.

[24] L. C. Gunderson and G. T. Holmes, "Microwave Luneburg lens," *Appl. Opt.*, vol. 7, no. 5, pp. 801–804, May 1968.

[25] X. Wu and J. J. Laurin, "Fan-beam millimeter-wave antenna design based on the cylindrical Luneberg lens," *IEEE Trans. Antennas Propag.*, vol. 55, no. 8, pp. 2147–2156, Aug 2007.

[26] A. Jouade, S. Meric, O. Lafond, M. Himdi, and L. Ferro-Famil, "A passive compressive device associated with a luneburg lens for multibeam radar at millimeter wave," *IEEE Antennas and Wireless Propagation Letters*, vol. 17, no. 6, pp. 938–941, June 2018.

[27] R. K. Luneburg, *Mathematical Theory of Optics*, 1944.

[28] R. F. Rinehart, "A family of designs for rapid scanning radar antennas," *Proc. IRE*, vol. 40, no. 6, pp. 686–688, June 1952.

[29] R. C. Mitchell-Thomas, O. Quevedo-Teruel, T. M. McManus, S. A. R. Horsley, and Y. Hao, "Lenses on curved surfaces," *Opt. Lett.*, vol. 39, no. 12, pp. 3551–3554, Jun 2014.

[30] Q. Liao, N. Fonseca, and O. Quevedo-Teruel, "Compact multibeam fully-metallic geodesic Luneburg lens antenna based on non-Euclidean transformation optics," *submitted to IEEE Trans. Antennas Propag.*, 2018.

[31] K. S. Kunz, "Propagation of microwaves between a parallel pair of doubly curved conducting surfaces," *J. Appl. Phys.*, vol. 25, no. 5, pp. 642–653, 1954.
[32] S. Maci, G. Minatti, M. Casaletti, and M. Bosiljevac, "Metasurfing: Addressing waves on impenetrable metasurfaces," *IEEE Antennas Wireless Propag. Lett.*, vol. 10, pp. 1499–1502, 2011.
[33] K. Liu, F. Ghasemifard, and O. Quevedo-Teruel, "Broadband metasurface Luneburg lens antenna based on glide-symmetric bed of nails," in *2017 11th European Conference on Antennas and Propagation (EUCAP)*, March 2017, pp. 358–360.
[34] L. Xue and V. F. Fusco, "Printed holey plate luneburg lens," *Microw. Opt. Technol. Lett.*, vol. 50, no. 2, pp. 378–380, 2007.
[35] ——, "24 GHz automotive radar planar Luneburg lens," *IET Microwaves Antennas Propag.*, vol. 1, no. 3, pp. 624–628, June 2007.
[36] A. Torki, M. Ebrahimpouri, and O. Quevedo-Teruel, "A planar steerable 60 GHz leaky wave antenna with Luneburg lens feed," in *2016 IEEE International Symposium on Antennas and Propagation (APSURSI)*, June 2016, pp. 1405–1406.
[37] A. Algaba-Brazalez, L. Manholm, M. Johansson, O. Quevedo-Teruel, and J. Miao, "Investigation of a Ka-band Luneburg lens made of a glide-symmetric holey structure," in *2017 International Symposium on Antennas and Propagation (ISAP)*, Oct 2017, pp. 1–2.
[38] J. Miao, *Ka-band 2D Luneburg Lens Design with Glide-symmetric Metasurface*. MSc Thesis, KTH Royal Insitute of Technology, 2017.
[39] G. Peeler and D. Archer, "A two-dimensional microwave Luneberg lens," *IRE Trans. Antennas Propag.*, vol. 1, no. 1, pp. 12–23, July 1953.
[40] C. Pfeiffer and A. Grbic, "A printed, broadband Luneburg lens antenna," *IEEE Trans. Antennas Propag.*, vol. 58, no. 9, pp. 3055–3059, Sept 2010.
[41] H. Legay, S. Tubau, E. Girard, J. P. Fraysse, R. Chiniard, C. Diallo, R. Sauleau, M. Ettorre, and N. Fonseca, "Multiple beam antenna based on a parallel plate waveguide continuous delay lens beamformer," in *2016 International Symposium on Antennas and Propagation (ISAP)*, Oct 2016, pp. 118–119.
[42] N. Kundtz and D. Smith, "Extreme-angle broadband metamaterial lens," *Nat. Mater.*, no. 9, pp. 129–132, 2010.
[43] O. Quevedo-Teruel, W. Tang, and Y. Hao, "Isotropic and nondispersive planar fed luneburg lens from Hamiltonian transformation optics," *Opt. Lett.*, vol. 37, no. 23, pp. 4850–4852, Dec 2012.
[44] S. Stein, "On cross coupling in multiple-beam antennas," *IRE Transactions on Antennas and Propagation*, vol. 10, no. 5, pp. 548–557, September 1962.
[45] H. Legay, E. Girard, G. Valerio, M. Ettorre, A. Ali, and R. Sauleau, "A large imaging array in Ka band with a substrate integrated waveguide pillbox beamformer," in *2014 IEEE Conference on Antenna Measurements Applications (CAMA)*, Nov 2014, pp. 1–4.